Spectral Zeeman hole burning in a quantum dot ensemble

Gang Chen,[1,*] E. T. Batteh,[1] D. G. Steel,[1] D. Gammon,[2] and D. S. Katzer[2]
[1]*Harrison M. Randall Laboratory of Physics, The University of Michigan, Ann Arbor, Michigan 48109-1120, USA*
[2]*The Naval Research Laboratory, Washington DC 20375, USA*
(Received 9 April 2003; published 11 September 2003)

Spectral hole burning experiments based on high-resolution magneto-CW four-wave mixing in the phase conjugate geometry show that both the spectral and spatial diffusion of excitons is negligible in the GaAs quantum dot system formed by interface disorder. Due to the strong Coulomb coupling, Zeeman spectral hole burning is observed when we resonantly excite one of the two orthogonally polarized excitons confined to each dot by two copolarized and frequency-degenerate fields and then probe the system by a third beam that is of opposite polarization and a Zeeman splitting away (in frequency). The experiments allow for a measure of the exciton decay rates and *g* factor.

DOI: 10.1103/PhysRevB.68.115303 PACS number(s): 71.35.Ji, 78.67.Hc

I. INTRODUCTION

GaAs quantum dots (QD's) naturally formed by interface disorder are among the most extensively investigated semiconductor nanostructure systems that show three-dimensional (3D) confinement of optically created excitons. Because of the Pauli exclusion principle and the discreteness of the electronic levels of each individual QD's, the linear and coherent nonlinear optical response from this system[1–11] is well described within the theoretical frame of atomic physics. These properties have been regarded as the basis for quantum information processing based on optically driven QD's.[12–15]

Single QD measurements based on submicron spatial resolution achieved by various means, however, cover only a relatively small subset of all QD's in the sample. An explicit spectroscopic study showing that most excitons are indeed localized and well isolated without suffering significant spatial and spectral diffusion is not yet available and is one of the main subjects of this paper. The experiments are based on probing an ensemble of QD's using high spectral resolution CW four-wave mixing (FWM) in the phase conjugate geometry.

FWM allows us to quickly study the exciton localization without relying on performing a large number of time-consuming single QD measurements or imaging each individual QD based on sophisticated near-field scanning microscopy.[5,16] The FWM technique is background free and both the frequency and polarization of all incident beams can be flexibly controlled. As will be detailed in this paper, this flexibility combined with an external static magnetic field allows for an observation of a conventional as well as a nonconventional Zeeman spectral hole burning (SHB) of magneto excitons. The data quantify the spectral and spatial diffusion of excitons and also (i) reveals an interesting inter-dot energy exchange process that is difficult to obtain in single QD studies; (ii) affirms that the excitons confined to each individual QD are strongly correlated by the Coulomb interaction, as expected;[8] (iii) demonstrates the importance of optically induced Zeeman coherence;[7,17] and (iv) measures the exciton decay dynamics as well as the *g* factor.[4]

Experiments are performed on an ensemble of natural dots in a 42-Å molecular beam epitaxy (MBE)-grown GaAs layer (with 250 Å $Al_{0.3}Ga_{0.7}As$ barriers).[3] The growth interruption at the $GaAs/Al_{0.3}Ga_{0.7}As$ interface leads to disorder with size comparable to the exciton Bohr diameter in GaAs, giving rise to quantum confinement in the lateral direction. Combined with the quantum confinement in the growth direction, the exciton states of each QD become fully discrete. This paper is concerned with the lowest bright heavy-hole exciton states which are twofold spin degenerate for dots that are circular in the lateral direction. Each of these excitons in a dot can be created by a resonant polarized optical field that excites one electron from the *p*-like heavy hole levels into the *s*-like conduction levels as shown in Fig. 1(a)[6–9] (the degeneracy of the conduction and heavy hole levels is removed for general cases, see the following discussion).

Gammon *et al.*[18] have shown that the two lowest heavy hole exciton transitions in these samples are linearly instead of circularly polarized due to the QD asymmetry. The external magnetic field applied in the Faraday configuration restores the selection rules to σ_+ and σ_- circular polarization.[4] The magnetic field also splits the conduction and heavy hole levels by different amounts and therefore induces a Zeeman splitting between the σ_+ and σ_- transitions as shown in Fig. 1(a).

An equivalent model in the excitation representation is shown in Fig. 1(b), with the crystal ground, the σ_+ and σ_- exciton states denoted by $|g\rangle$, $|+\rangle$, and $|-\rangle$. The Coulomb interaction between the two excitons can be easily incorpo-

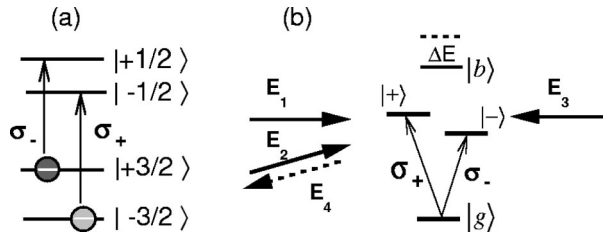

FIG. 1. (a) Diagram for relevant energy levels of a single GaAs QD and the two optically allowed exciton transitions. (b) An equivalent model in the excitation representation. The ground, exciton, and biexciton states are denoted by $|g\rangle$, $|\pm\rangle$, and $|b\rangle$. Phase-conjugate FWM setup is also shown.

rated in this basis and is represented by the energy shift ΔE of the biexciton state (the biexciton binding energy). Symbols γ_{ij} and Γ_{ij} denote the dephasing and energy relaxation rates between level i and j ($i \neq j$), respectively. Evidence for biexcitons in this system (with $\Delta E \sim 3$ meV) was reported elsewhere.[8,10,19] Both the homogeneous and inhomogeneous linewidths of the QD excitons are at least one order of magnitude smaller than the typical ΔE. Thus, by tuning the CW lasers to excite the exciton states, the contribution from level $|b\rangle$ is negligible.

The overall optical response of a QD ensemble is an integration over many dots whose exciton energies lie sufficiently close to that of the excitation fields. The sample is placed in a magnetic cryostat at 5 K. All CW lasers are frequencies stabilized to ~ 4 neV with a mutual coherent bandwidth of ~ 20 neV.

II. PHASE CONJUGATE FWM

The phase conjugate FWM geometry is shown in Fig. 1(b)[20] with three incident fields denoted by $\mathbf{E}_n$, abbreviation for $\mathbf{E}_n(\mathbf{k}_n, \Omega_n)$. Here, $n=1,2,$ or 3 and $\mathbf{k}$ and Ω denote the wave vector and angular frequency of the fields, respectively. The two counterpropagating fields $\mathbf{E}_1$ and $\mathbf{E}_3$ ($\mathbf{k}_1 = -\mathbf{k}_3$) intersect $\mathbf{E}_2(\Omega_2)$ on the sample. The coherent nonlinear optical emission $\mathbf{E}_4$ with a $\mathbf{k}$ vector opposite to $\mathbf{E}_2$ ($\mathbf{k}_4 = -\mathbf{k}_2$) is a combination of the contributions from the Bragg scattering of $\mathbf{E}_3$ off the front excitation grating due to the spatial and temporal modulation of excitons by $\mathbf{E}_1\mathbf{E}_2^*$, and a similar process involving the back grating created by $\mathbf{E}_2^*\mathbf{E}_3$ which scatters $\mathbf{E}_1$ into $-\mathbf{k}_2$ direction.

In the weak-field limit, both contributions come from the various terms in the third-order polarization of the form $P_4^i = \Sigma_{jkl}\chi_{(3)}^{ijkl}(\Omega_4;\Omega_1,-\Omega_2,\Omega_3)E_1^j E_2^{*k} E_3^l + \text{c.c.}$ Here the indices $ijkl$ refer to the Cartesian components of the fields and $\chi_{(3)}^{ijkl}$ represents the third-order suseptibility tensor which can be solved perturbatively using the equations of motion of the density matrix.[21] The frequency of the signal is determined by $\Omega_4 = \Omega_1 - \Omega_2 + \Omega_3$. The $\mathbf{E}_4$ field is detected by a square-law photodetector leading to a signal proportional to $|\mathbf{P}_4|^2$.

Each field is made either σ_+ or σ_- polarized[22] using a linear polarizer and a quarter-wave plate in our experiments so that it only excites one of the two exciton transitions and greatly reduces the number of terms in the third-order polarization $\mathbf{P}_4$. Two fields of the same polarization create population gratings of corresponding excitons. Two beams of orthogonal polarization allow for the coupling of the $|+\rangle$ and $|-\rangle$ states via the crystal ground state $|g\rangle$. This creates a spatial modulation of exciton coherence that involves both excitons and is equivalent to a coherent superposition of the $|+\rangle$ and $|-\rangle$ states, the Zeeman coherence.[7,17] It is spatially modulated (due to the interference pattern between the excitation fields) to form the Zeeman coherence grating. Both types of gratings discussed above can be either front or back gratings. Thus, by adjusting the polarization of the incident fields, different contributions can be selectively studied.

Furthermore, the three incident fields can be independently tuned in frequency and three types of experiments are considered in this paper.[23] In type-I experiments, all beams are degenerate in frequency and tuned. In type-II experiments, we keep Ω_1 and Ω_2 the same and fixed and tune Ω_3 with a detuning of $\delta_{3,12}$ (representing frequency difference between Ω_3 and Ω_1/Ω_2). In this case, the front grating is stationary leading to a contribution to the FWM signal that is sensitive to only the dephasing rate $\gamma_{\alpha g}$, where $\alpha = +$ or $-$. The back grating, however, moves in the plane of the sample at a speed determined by $\delta_{3,12}$. Its contribution is sensitive to both the dephasing rates $\gamma_{\alpha g}$ and energy relaxation rates $\Gamma_{\alpha g}$.[23] In type-III experiments, however, Ω_1 and Ω_3 are fixed at the same value but Ω_2 is scanned with a detuning of $\delta_{2,13}$. In this case, both gratings move and their contributions to the FWM signal depend identically on $\gamma_{\alpha g}$ and $\Gamma_{\alpha g}$.[23]

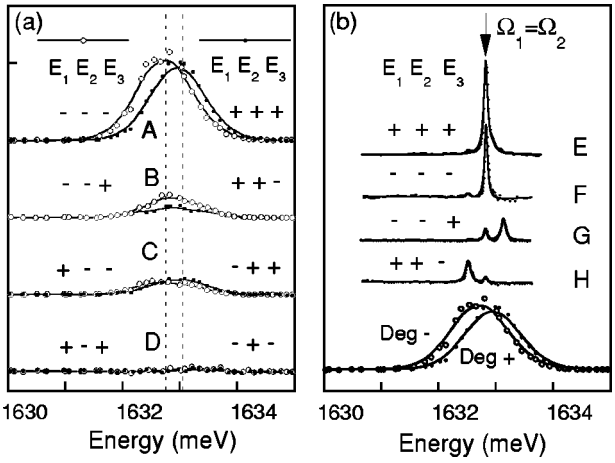

FIG. 2. (a) Degenerate FWM spectra at 4.3 T under all possible polarization configurations. (b) Type-II nondegenerate FWM spectra under various polarization configurations. $\mathbf{E}_1$ and $\mathbf{E}_2$ are fixed at 1632.82 meV, as indicated by the arrow. The bottom curves are degenerate FWM spectra. The energy axis represents $\hbar\Omega_3$.

Considering the inhomogeneous broadening, a degenerate type-I spectrum maps out the absorption profile of all dots. In a nondegenerate type-II or -III experiment, however, the two beams fixed in frequency only excite one group of QD's that are resonant, leading to the removal of inhomogeneous broadening and spectral hole burning. Results from these three types of experiments will be presented in next section.

III. RESULTS AND DISCUSSIONS

A. Polarization Sensitive Degenerate FWM

We first focus on polarization sensitive degenerate (type I) FWM spectra shown in Fig. 2(a). The data were taken at 4.3 T with all possible polarization combinations of the three fields. In curves A, all beams are circularly polarized with the same direction of rotation and thus excite only the σ_+ or σ_- exciton state in each QD. The curves show the inhomogeneously broadened exciton response with the energy difference between the σ_+ and σ_- curves being the Zeeman splitting, Δ_z in frequency units. The third-order polarization terms causing this FWM signal are due to excitation following the perturbation path given by[17]

$$\rho_{g,g} \rightarrow^{\mathbf{E}_2^*(\sigma_\alpha)}_{\mathbf{E}_2^*(\sigma_\alpha)} \rho_{\alpha,g} \rightarrow^{\mathbf{E}_2^*(\sigma_\alpha)}_{\mathbf{E}_2^*(\sigma_\alpha)} (\rho_{\alpha,\alpha} - \rho_{g,g}) \rightarrow^{\mathbf{E}_3(\sigma_\alpha)}_{\mathbf{E}_1(\sigma_\alpha)} \rho_{\alpha,g}, \quad (1)$$

where the upper and lower paths are the front and back exciton population grating contributions, respectively. The polarization of each beam is indicated in the bracket and the subscript α represents either $+$ or $-$.

The FWM signal is predicted to be absent based on the model of Fig. 1(b) when $\mathbf{E}_1$ and $\mathbf{E}_3$ are co-circularly polarized and $\mathbf{E}_2$ is of orthogonally circular polarization.[17] Curves D in Fig. 2(a) agree with this prediction. This confirms that with the magnetic field applied in the Faraday configuration the exciton transitions are indeed circularly polarized because any deviation from the circular selection rules would result in nonzero signal.

For the polarization configuration that leads to curves B, the excitation of the $|\alpha\rangle$ exciton by the σ_α polarized $\mathbf{E}_1$ and $\mathbf{E}_2$ leads to a front ground-state population grating, which then causes the scattering of the σ_β $(\alpha \neq \beta)$ polarized $\mathbf{E}_3$ via the $|\beta\rangle$ exciton transition. The perturbation chain is the upper path (we will discuss the lower path later):[17]

$$\rho_{g,g} \rightarrow^{\mathbf{E}_1(\sigma_\alpha)}_{\mathbf{E}_3(\sigma_\alpha)} \rho_{\alpha,g} \rightarrow^{\mathbf{E}_2^*(\sigma_\alpha)}_{\mathbf{E}_2^*(\sigma_\alpha)} \rho_{g,g} \rightarrow^{\mathbf{E}_3(\sigma_\beta)}_{\mathbf{E}_1(\sigma_\beta)} \rho_{\beta,g}. \quad (2)$$

The back grating of curves B, however, is due to the Zeeman coherence created by the cross polarized $\mathbf{E}_2$ and $\mathbf{E}_3$ which follows the lower path:

$$\rho_{g,g} \rightarrow^{\mathbf{E}_1(\sigma_\alpha)}_{\mathbf{E}_3(\sigma_\alpha)} \rho_{\alpha,g} \rightarrow^{\mathbf{E}_2^*(\sigma_\beta)}_{\mathbf{E}_2^*(\sigma_\beta)} \rho_{\alpha,\beta} \rightarrow^{\mathbf{E}_3(\sigma_\beta)}_{\mathbf{E}_1(\sigma_\beta)} \rho_{\alpha,g}. \quad (3)$$

The vectorial characteristics of the signal $\mathbf{E}_4$ should be the same as that of the field $\mathbf{E}_2$,[17] in either case, which was experimentally confirmed.

However, neither the ground state nor Zeeman coherence grating contribution to curves B is fully resonant for degenerate beams because the Zeeman splitting is about 3.5 times larger than the exciton linewidth (the exciton linewidth was measured in Ref. 6 and will be discussed in Sec. III D), leading to a reduction of the signal roughly by a factor of $[(\gamma + \Delta_z)/\gamma]^2 \simeq 20$ from the resonant case (curves A). The signal in B is clearly larger than expected and is attributed to an interdot energy transfer from the $|\alpha\rangle$ exciton population grating to form an energetically degenerate $|\beta\rangle$ excitons grating, which then scatters the σ_β polarized $\mathbf{E}_3$. This is evident by noting that the spectral position of the σ_α grating contribution in curve B is correlated with the σ_α curve in A. As will be shown later, interdot spectral diffusion (higher energy to lower energy relaxation) is negligible. The data here show that the interdot energy transfer rate becomes significant when the initial and final states are nearly degenerate. The resonant enhancement of the energy-transfer process was also observed in wide GaAs quantum wells.[24]

Curves C can be explained in a similar way to curves B except that the front grating becomes a Zeeman coherence grating following the upper path of Eq. (3) and the back grating is a ground-state population grating following the lower path of Eq. (2).

B. Spectral Hole Burning

We now turn to the nondegenerate FWM type-II experiments. The fixed Ω_1/Ω_2 leads to the removal of inhomogeneous broadening and spectral hole burning. By arranging the polarization of the beams, it is possible to detect the excitation of the σ_α polarized exciton states via the σ_β states, leading to a Zeeman spectral hole burning.

Type-II spectra at 4.3 T is shown in Fig. 2(b) as a function of $\hbar\Omega_3$. Ω_1 and Ω_2 are fixed at the position indicated by the arrow. With all beams σ_α polarized (E and F), strong spectral hole burning is observed at $\hbar\Omega_1 = \hbar\Omega_2$. Both the front and back gratings contribute, following the perturbation chains of Eq. (1). In the case of σ_+ polarized $\mathbf{E}_1$ and $\mathbf{E}_2$, and σ_- polarized $\mathbf{E}_3$, as shown in Fig. 2(b) H, we observe a strong hole due to the Zeeman split states Δ_z away from the fixed $\hbar\Omega_1$ and $\hbar\Omega_2$. This hole is a result of a front population grating following the upper path in Eq. (2) and a back Zeeman coherence grating following the lower path in Eq. (3). The small signal at $\hbar\Omega_1$ is attributed to the resonant energy transfer discussed previously. A similar result is obtained using σ_+ polarized $\mathbf{E}_2$ and $\mathbf{E}_3$, and σ_- polarized $\mathbf{E}_1$ (not shown). In this case, the back (population) and front (Zeeman coherent) gratings follow the lower path of Eq. (2) and upper path of Eq. (3), respectively.

The result obtained with σ_- polarized $\mathbf{E}_1$ and $\mathbf{E}_2$ and σ_+ polarized $\mathbf{E}_3$ is shown in curve G of Fig. 2(b). It is similar to H except that the Zeeman hole is on the other (higher energy) side of Ω_1, as expected. The measurement (not shown) using σ_- polarized $\mathbf{E}_2$ and $\mathbf{E}_3$ and σ_+ polarized $\mathbf{E}_1$ yields an identical spectrum with the spectral hole on the higher energy side.

We note that according to Eq. (1), both the $|g\rangle$ and $|\alpha\rangle$ population contributes to the holes in E and F of Fig. 2 when all three fields are co-polarized. Considering both the front and back gratings, there are four contributing terms to the signal. On the other hand, the Zeeman hole in G and H contains only the ground-state population path in Eq. (2) and one path in Eq. (3), a total of two terms. Since the FWM signal is proportional to $|\mathbf{P}_4|^2$, we expect that the holes in E and F to be roughly four times stronger than the Zeeman hole in G and H. The experimental data agree with this speculation.

The exciton g factor of -1.2 can be obtained in a straightforward way from the Zeeman splitting determined by the above hole burning experiments. We find that the Zeeman splitting satisfies $\hbar\Delta_z = g\mu_B B$ up to 5 T. Here, μ_B is the Bohr magneton. Both the sign and magnitude of the exciton g factor measured here are consistent with Ref. 25, which shows that for a 42-Å quantum well (QW) structure, the electron g factor is slightly positive (the $+1/2$ level is higher in energy than the $-1/2$ level) but the hole g factor is negative (the $+3/2$ level is higher than the $-3/2$ level), leading to a negative exciton g factor. Compared to degenerate FWM which also allows for measuring the g factor, an advantage of the type-II nondegenerate experiments is that Ω_1 and Ω_2 can be tuned to various spectral position and the g factor of excitons as a function of energy can be studied. We did not observe any notable dependence. Interestingly, the

linewidth of the Zeeman hole in Fig. 2(b) G and H is about 1.8 times larger than that of the spectral holes in E and F. This could be due to a large decay rate of the Zeeman coherence. However, from the single QD studies discussed in Ref. 7, we know that the Zeeman coherence decay rate is comparable to that of the exciton dipole coherence and is unlikely to cause a broadening of the Zeeman spectral holes. Alternatively, if the exciton g factor is inhomogeneously distributed, we expect to see a broadening of the Zeeman holes. The variation of the exciton g factor was indeed observed in single QD studies.[26] Assuming a Gaussian distribution of the g factor, it can be shown that the broadening of the Zeeman holes corresponds to a g variation of ± 0.2. The g factor distribution is a manifestation of the variation of the local environment of each individual QD (such as the size and shape of the dots).

C. Higher-Order Coulomb Correlation

The Zeeman hole burning originates from different physics compared to that observed in GaAs quantum wells (QW's).[24] First, the probed Zeeman hole in wide QW's was due to the spin-flip of excitons. Only a Zeeman hole on the lower energy side was observed, an indication of energy relaxation as the physical origin. Second, it was measured that the amplitude of that hole decreases dramatically with the increasing magnetic field, which reduces the spin-flip rate. In our measurements discussed in the previous section, however, Zeeman holes on both sides of $\hbar\Omega_1$ and $\hbar\Omega_2$ are observed, which cannot be explained by spin flip alone at low temperatures. According to Refs. 3, 7, 27, and 28, the spin relaxation rate in this QD system is small and can be neglected. In addition, the signal strength of the Zeeman holes relative to the holes in E and F of Fig. 2 is found to be independent of the magnetic field.

The Zeeman hole burning in the interface QD system is caused by the same physics discussed in Ref. 7. In particular, the σ_+ and σ_- excitons confined to each dot are strongly correlated by the Coulomb interaction. Thus the excitation of one exciton leads to a nonzero grating in the other exciton transition and two fields that are Δ_z apart can jointly create a Zeeman coherence grating of two excitons. The Coulomb coupling shifts the $|\alpha\rangle \rightarrow |b\rangle$ transition off resonance with any beam so that the scattering by coupling to the biexciton state is negligible. Without the Coulomb coupling, this scattering would cancel the contribution of Eq. (2), leading to zero net contribution to the Zeeman hole. In Ref. 8, we have confirmed that the Coulomb correlation energy is around 3.5 meV, much larger than both the homogenous and inhomogeneous linewidths of the excitons of concern.

D. Spectral Diffusion, Exciton Lifetime, and Dephasing

The SHB experiments discussed above can provide information regarding the exciton relaxation dynamics and the spectral diffusion of excitons as well. In the early SHB measurements made in wide GaAs quantum wells,[29,30] it was found that the spectral diffusion from high- to low-energy excitons leads to a substantial tail in addition to the sharp spectral hole on the lower energy side. This is because the spectral diffusion due to energy transfer leads to the formation of exciton gratings at lower energies, which is then probed by tuning E_3 to these energies. From curves E and F of Fig. 2(b), it is apparent that the spectral diffusion of excitons to the lower energy states is negligible within the experimental uncertainty in the studied structures. This is possibly due to the enhanced separation and consequently reduced interaction between excitons localized at different sites.

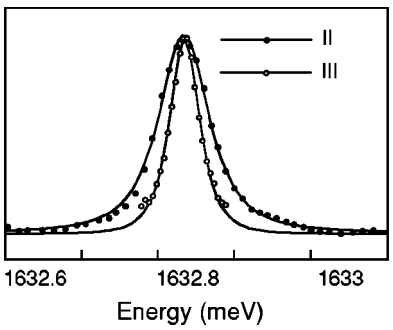

FIG. 3. Comparison of type-II and -III nondegenerate FWM spectra at 4.3 T. All beams are σ_+ polarized. The beams with fixed frequency are at 1632.82 meV. The solid lines are curve fitting based on Eqs. (4) and (5). Similar results were obtained with all beams σ_- polarized.

From the copolarized type-II FWM spectra, the exciton decay rates can be extracted. For E and F of Fig. 2(b), a calculation following Eq. (1) yields that the signal is

$$I_{II} \propto \frac{|E_1 E_2 E_3|^2 |\mu_{g\alpha}|^8}{W^2(4\gamma_{\alpha g}^2 + \delta_{3,12}^2)} \left(\frac{1}{\Gamma_{\alpha g}^2} + \frac{3}{\Gamma_{\alpha g}^2 + \delta_{3,12}^2} \right), \qquad (4)$$

where the first term is purely from the front grating, one-third of the second term is from the back grating, and two-thirds of the second term is the interference between the gratings (when taking a modulus square of the polarization). The ensemble average is taken by integrating over all dots, assuming a Gaussian distribution with width W. Due to the contribution from all dots whose resonance frequency is near Ω_1 and Ω_2, the line shape of the signal is characterized by $2\gamma_{\alpha g}$ (instead of $\gamma_{\alpha g}$) and $\Gamma_{\alpha g}$. The overall line shape is complex compared to the bulk GaAs case, where the back grating can be neglected and only the first term in Eq. (4) remains, giving rise to a simple Lorentzian characterized by 2γ. This is because the back grating is closely spaced and the strong exciton migration (spatial diffusion) in bulk GaAs washes out this grating. However, this is not the case in the present system (see later discussion on spatial diffusion).

A curve fitting of Fig. 2(b) E is shown in Fig. 3, yielding $\gamma_{+g}^{-1} = 25 \pm 3$ and $\Gamma_{+g}^{-1} = 11 \pm 2$ ps. Similar results are obtained for γ_{-g} and Γ_{-g}. These values are consistent with single QD measurements.[6,8,10] From these numbers, we conclude that the pure dephasing of excitons due to phase changing scattering events is insignificant, again, in support of the reduced elastic scattering of excitons due to localization. At the ensemble level, our measurements show that this is true for majority of the QD's.

The line shape of the Zeeman hole in curves G and H of Fig. 2(b) carries the information about the decay rate of the Zeeman coherence, γ_{+-}. However, as shown in earlier discussions, the inhomogeneity of the exciton g factor of the ensemble significantly modifies the linewidth of the Zeeman holes and thus makes the measurement of γ_{+-} impossible in these experiments. The single QD studies discussed in Ref. 26 show that γ_{+-} is mostly caused by the decay of excitons (rates γ_{+g} and γ_{-g}); the excess dephasing of the Zeeman coherence beyond the part determined by the exciton dephasing is less than the exciton dephasing itself.

E. Spatial Diffusion of Excitons

Finally, we address co-polarized type-III nondegenerate FWM experiments, compare them with type-II measurement, and discuss how to extract information on the spatial diffusion of excitons.

For copolarized type-III FWM, both the front and back traveling gratings that follow Eq. (1) contribute identically to the total signal,

$$I_{III} \propto \frac{|E_1 E_2 E_3|^2 |\mu_{g\alpha}|^8}{W^2(\Gamma_{\alpha g}^2 + \delta_{2,13}^2)(\gamma_{\alpha g}^2 + \delta_{2,13}^2)}. \tag{5}$$

The line shape is a product of two Lorentzians characterized by $\Gamma_{\alpha g}$ and $\gamma_{\alpha g}$. In bulk GaAs, due to the strong pure dephasing of excitons, $\gamma_{\alpha g}$ is much larger than the $\Gamma_{\alpha g}$ so that the signal is very well approximated by the narrower Lorentzian with width $\Gamma_{\alpha g}$. In the QD system under study, this assumption is not valid (see Ref. 6 and the earlier discussions on the exciton decay rates based on type-II measurements). A type-III spectrum obtained using σ_+ polarized beams is shown by the open circles in Fig. 3. Ω_1 and Ω_3 are fixed at the center of the spectrum. It is obviously narrower than the type-II spectrum (solid circles) because the ensemble average does not impose a factor of 2 in front of γ_{+g}. Fitting the type-III spectrum to Eq. (5) yields $\gamma_{+g}^{-1} = 25 \pm 2$ ps and $\Gamma_{+g}^{-1} = 11 \pm 2$ ps, in excellent agreement with the type-II results discussed in the previous section.

It is assumed so far in all the theoretical analysis above that the spatial diffusion of excitons is negligible due to the relatively strong exciton localization. Simple experiments based on traveling grating excitation can be used to study the exciton transport and to confirm this assumption.[31–33] For example, in the type-III experiments, the grating spacing is controlled by varying the angle θ between the **k** vectors of $\mathbf{E}_1$ and $\mathbf{E}_2$. The effect of the spatial diffusion process is to reduce the contrast of the excitation gratings and is equivalent to an effective increase of Γ that depends on the diffusion coefficient. This effective change of Γ would affect the linewidth of the type-III spectra. Under the diffusive limit and using the appropriate diffusion equation for the excited-state density, Ref. 31 showed that the total effective energy relaxation rate Γ_{total} including the effect of the spatial diffusion is

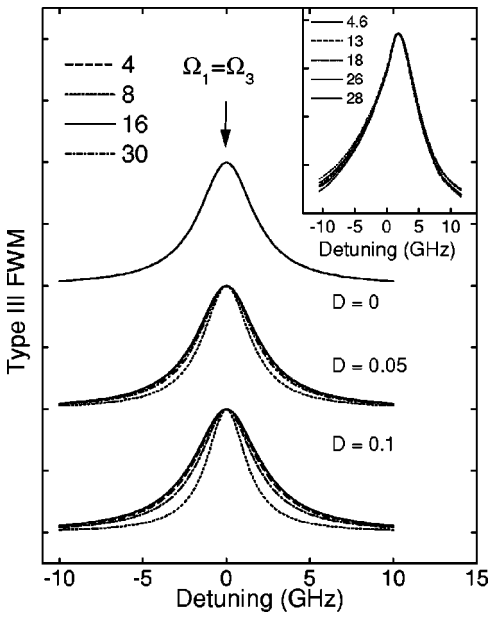

FIG. 4. Calculated type-III FWM spectra as a function of θ with various exciton diffusion coefficient D, which is in units of cm^2/s. The angle θ is in units of degree. When D is zero, the spectra are independent of θ. The experimental results are plotted in the inset.

$$\Gamma_{total} = \Gamma + 4\pi^2 D/\Lambda^2, \tag{6}$$

where D is the diffusion coefficient of excitons and Λ is the grating spacing determined by

$$\Lambda = \frac{\lambda}{2n \sin(\theta/2)} \tag{7}$$

for the front grating and by

$$\Lambda = \frac{\lambda}{2n \sin\left(\frac{\pi - \theta}{2}\right)} \tag{8}$$

for the back grating. Here, λ is the wavelength of the excitation optical field in vacuum and n is the index of refraction of the material.

Figure 4(a) shows the predicted type-III spectra as a function of θ assuming various values for the exciton spatial diffusion coefficient D. The theory suggests that the line shape has a strong angle dependence even for D as small as 0.05 cm^2/s. From the experimental data shown in the inset of Fig. 4 (θ is varied between 4° and 30° in the lab), we conclude that the exciton spatial diffusion is smaller than 0.05 cm^2/s in the system under study, which is at least three orders of magnitude smaller than that of bulk GaAs.[33] Our experiments show a simple way to verify that the excitons are indeed localized in these structures without relying on sophisticated near-field imaging techniques.

IV. CONCLUSION

To conclude, we show in this paper, by using high spectral resolution magneto-FWM, the absence of both spectral and spatial diffusion of excitons localized in the GaAs QD's formed by interface disorder. The Zeeman hole burning experiments suggest that the two lowest energy excitons confined to each dot are strongly correlated by the Coulomb interaction. These studies also provide a measure of exciton decay rates and *g* factor.

ACKNOWLEDGMENTS

This work was supported in part by the National Security Agency (NSA) and Advanced Research and Development Activity (ARDA) under Army Research Office (ARO) Contract No. DAAG55-98-1-0373, by the Air Force Office of Scientific Research (AFOSR) under Grant No. F49620-99-1-0045, and by DARPA/Spins. D.G.S. thanks the Guggenheim Foundation for financial support.

*Currently at: Bell Labs, Lucent Technologies, Murray Hill, NJ 07974.

[1] K. Brunner, U. Bockelmann, G. Abstreiter, M. Walther, G. Böhm, G. Tränkle, and G. Weimann, Phys. Rev. Lett. **76**, 3216 (1992).
[2] H.F. Hess, E. Betzig, and T.D. Harris, Science **264**, 1740 (1994).
[3] D. Gammon, E.S. Snow, B.V. Shanabrook, D.S. Katzer, and D. Park, Science **273**, 87 (1996).
[4] S.W. Brown, T.A. Kennedy, D. Gammon, and E.S. Snow, Phys. Rev. B **54**, R17 339 (1996).
[5] Q. Wu, R.D. Grober, D. Gammon, and D.S. Katzer, Phys. Rev. Lett. **83**, 2652 (1999).
[6] N.H. Bonadeo, G. Chen, D. Gammon, D.S. Katzer, D. Park, and D.G. Steel, Phys. Rev. Lett. **81**, 2759 (1998).
[7] G. Chen, N.H. Bonadeo, D.G. Steel, D. Gammon, D.S. Katzer, D. Park, and L.J. Sham, Science **289**, 1906 (2000).
[8] G. Chen, T.H. Stievater, E.A. Tabak, X. Li, D.G. Steel, D. Gammon, D.S. Katzer, D. Park, and L.J. Sham, Phys. Rev. Lett. **88**, 117901 (2002).
[9] T.H. Stievater, X. Li, D.G. Steel, D.S. Katzer, D. Park, D. Gammon, L.J. Sham, and C. Piermarocchi, Phys. Rev. Lett. **87**, 133603 (2001).
[10] T.H. Stievater, X. Li, D.G. Steel, D. Gammon, D. Park, and D.S. Katzer, Phys. Rev. B **65**, 205319 (2002).
[11] J.R. Guest, T.H. Stievater, X. Li, J. Cheng, D.G. Steel, D. Gammon, D.S. Katzer, D. Park, C. Ell, A. Thranhardt, G. Khitrova, and H.M. Gibbs, Phys. Rev. B **65**, 241310(R) (2002).
[12] A. Ekert and R. Jozsa, Rev. Mod. Phys. **68**, 733 (1996).
[13] A. Imamoğlu, D.D. Awschalom, G. Burkard, D.P. DiVincenzo, D. Loss, M. Sherwin, and A. Small, Phys. Rev. Lett. **83**, 4204 (1999).
[14] E. Biolatti, R.C. Iotti, P. Zanardi, and F. Rossi, Phys. Rev. Lett. **85**, 5647 (2000).
[15] P. Chen, C. Piermarocchi, and L.J. Sham, Phys. Rev. Lett. **87**, 067401 (2001).
[16] J.R. Guest, T.H. Stievater, G. Chen, E. Tabak, B. Orr, D.G. Steel, D. Gammon, and D.S. Katzer, Science **293**, 2224 (2001).
[17] J.F. Lam, D.G. Steel, and R.C. Lind, Appl. Phys. Lett. **38**, 977 (1981).
[18] D. Gammon, E.S. Snow, B.V. Shanabrook, D.S. Katzer, and D. Park, Phys. Rev. Lett. **76**, 3005 (1996).
[19] Q. Wu, R.D. Grober, D. Gammon, and D.S. Katzer, Phys. Rev. B **62**, 13 022 (2000).
[20] *Optical Phase Conjugation*, edited by R. A. Fisher (Academic Press, New York, 1983).
[21] I.M. Beterov and V.P. Chebotaev, Prog. Quantum Electron. **3**, 1 (1974).
[22] In this paper, the direction of rotation of the *E* field is with respect to the *z* axis of the magnetic field. The same rotations are considered copolarized.
[23] D.G. Steel and J.T. Remillard, Phys. Rev. A **36**, 4330 (1987).
[24] H. Wang, M. Jiang, R. Merlin, and D.G. Steel, Phys. Rev. Lett. **69**, 804 (1992).
[25] M.J. Snelling, E. Blackwood, C.J. McDonagh, R.T. Harley, and C.T. Foxon, Phys. Rev. B **45**, 3922 (1992).
[26] G. Chen, Ph.D. thesis, The University of Michigan, The Harrison M. Randall Laboratory of Physics, Ann Arbor MI, 2001.
[27] T. Takagahara, J. Lumin. **87-89**, 308 (2000).
[28] T. H. Stievater, X. Li, D. G. Steel, D. Gammon, D. S. Katzer, and D. Park (unpublished).
[29] H. Wang, M. Jiang, and D.G. Steel, Phys. Rev. Lett. **65**, 1255 (1990).
[30] H. Wang and D.G. Steel, Phys. Rev. A **43**, 3823 (1991).
[31] J.R. Salcedo, A.E. Siegman, D.D. Dlott, and M.D. Fayer, Phys. Rev. Lett. **41**, 131 (1978).
[32] D. Oberhauser, K.H. Pantke, J.M. Hvam, G. Weimann, and C. Klingshirn, Phys. Rev. B **47**, 6827 (1993).
[33] A.C. Schaefer, J. Erland, and D.G. Steel, Phys. Rev. B **54**, R11 046 (1996).